JOURNAL OF MATERIALS SCIENCE 20 (1985) 105–113

Rheological behaviour and microstructure of stir-casting zinc–aluminium alloys

H. LEHUY, J. MASOUNAVE, J. BLAIN
Industrial Materials Research Institute, National Research Council of Canada, 750 Bel-Air Street, Montreal, Quebec, Canada H4C 2K3

The influence of processing variables on the rheological and microstructural behaviour of stir-cast (rheocast) ZA-27 alloy (Zn–27 wt % Al–2 wt % Cu) has been investigated experimentally. A concentric cylinder viscometer with shear rate range up to 650 sec^{-1} was used to measure the apparent viscosity of the slurries. During continuous cooling and at high shear rates (300–640 sec^{-1}), non-dendritical materials obey the power-law fluid model, i.e. $\eta_a = k\dot{\gamma}^n$ where η_a is the apparent viscosity and $\dot{\gamma}$ the shear rate. At lower shear rates (125 sec^{-1}), the slurries display dendritical–liquid mixture with viscosity up to 50 poises. Microstructural studies of continuously cooled materials reveal a clear tendency of primary particles to cluster. This phenomenon could be explained by the reduction of the amount of entrapped liquid in the particles.

1. Introduction

There are many recent reports in the literature describing studies on the rheology of partially solid alloys and the application of the findings to innovative and improved casting and metal forming processes. Work has been reported on various alloys such as aluminium [1–3], magnesium [4], copper based alloys [5, 6], steel [7, 8] and superalloys [9, 10].

The fundamental point of this emerging solidification processing technique is vigorous agitation of a solidifying alloy by mechanical stirring from the time solidification starts until the metal is cast. Due to the thixotropic properties of the sheared slurry, the material viscosity is decreased so the alloy can flow smoothly. The thixotropic slurry can then be advantageously mould-cast [11, 12] or die-cast [13, 14]. The mechanical stirring breaks up the dendrites and creates a unique structure, where spherical or rosette shaped particles are suspended in the remaining liquid. The mechanisms causing this novel microstructure are not yet fully understood, although the mechanical fragmentation [15] of the solidifying dendrites has been proposed to explain the grain multiplication structure. More recently, "abnormal" subgrain boundaries of clustered particles have been observed in Al–Mg stir-cast alloy and they have been thought to grow by particle-coalescence or growth-twinning mechanisms [16].

The aims of this study are to determine how the technology relating to the casting of partially solid metals can be applied to Zn–Al alloys. The research is still in progress, and clustering effects of the primary particles are being observed. This paper describes some of the results obtained about the rheological behaviour and the microstructure of stir-casting Zn–Al alloys.

2. Experimental details

A zinc alloy with 27 wt % aluminium and 2 wt % copper was used for this study. This alloy commercially named ZA-27 was developed by Noranda Mines Ltd for casting applications. Its nominal composition and the liquidus and solidus temperatures are given in Table I. Also, in order to know the thermodynamic properties of this alloy, the specific heat and the solidification enthalpy were also measured with a high precision thermobalance and the results are presented in Fig. 1. These data were used in the design of our experiments and indicates the amount of heat to be extracted by the cooling system.

In order to prepare the ZA-27 alloy in the

0022–2461/85 $03.00 + .12

TABLE I Characteristics of the ZA-27 alloy

Alloy nomenclature	Nominal composition (wt %)			Temperature (° C)	
				Liquidus	Solidus
	Al	Cu	Zn		
ZA-27	25–28	2.0–2.5	Remainder	492 ± 5	437 ± 5

desired partially solid form, a "slurry machine" was constructed. This machine was modelled after the MIT apparatus [17] used for making thixotropic products with other alloys. The molten alloy was simultaneously stirred and cooled in the machine, and the partially solid product was delivered through the discharge end at a known controlled temperature. The crucible is made of high purity graphite and has a capacity of 10 kg of metal alloy. The agitator is made of stainless steel. To avoid contamination of the melt by iron, 0.5 mm of alumina was plasma-sprayed on the agitator shaft. Four thermocouples, TC, were inserted at different points in the apparatus; one of them, a chromel–alumel TC was placed just under the discharge nozzle to measure the temperature of the slurry flowing out of the machine. The casting rate was controlled either by the diameter of the nozzle hole or the gap between the nozzle and the agitator. For example, with a 6.4 mm diameter nozzle and a gap of 3.2 mm, zinc slurry can be continuously cast at a rate of 1 kg min^{-1}. The slurry was cast into 50.8 mm diameter graphite moulds. To prevent the quench phenomenon when the first slurry drops splash the graphite walls, the moulds were preheated to 400° C prior to being used. For most of the work done with zinc alloys, the solid fraction was in the range 0.2 to 0.6. Past the 0.6 solid fraction point the slurry was too viscous and sound ingots were difficult to obtain.

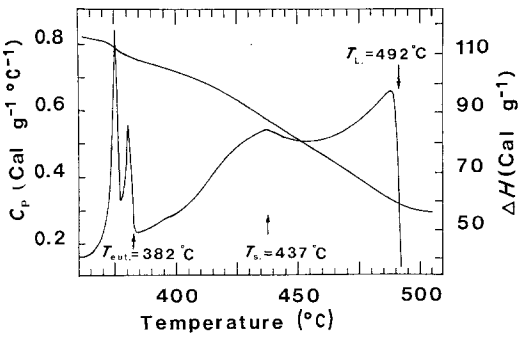

Figure 1 Specific heat and enthalpy of solidification of ZA-27 alloy, with starting temperature, $T_0 = 560°$ C and cooling rate, $G = 2°$ C min^{-1}.

3. Rheological behaviour

Both the temperature and the stirring speed, control the solid fraction of a thixotropic slurry and determine the apparent fluidity of the melt. In order to determine the rheological behaviour of slurries inside the rheocaster under operating conditions, an unconventional viscometer was designed. A schematic diagram of the apparatus is shown in Fig. 2 where a cylindrical spindle was rotated in a 28.6 mm diameter alumina crucible. A synchroelectric Brookfield viscometer equipped with a 25.4 mm diameter spindle was used to determine the viscosity of the slurries. The molten alloy was introduced into the preheated crucible then continuously cooled at a rate of 3° C min^{-1}. Thermocouples controlled the cooling temperature and an induction coil was used to preheat the apparatus and to maintain the temperature to

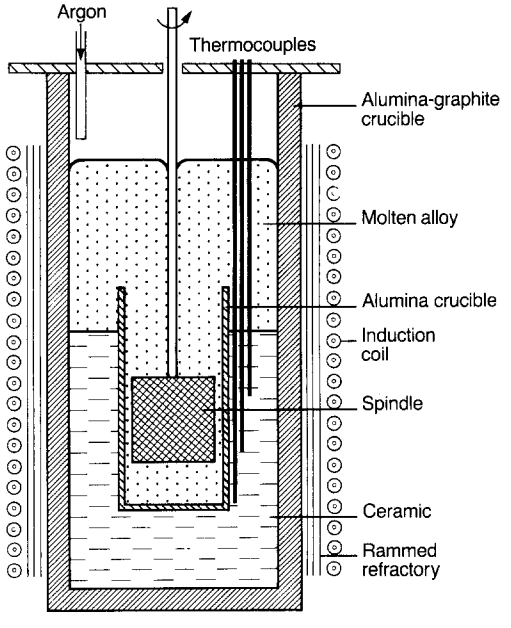

Figure 2 Schematic diagram of the apparatus for high-temperature viscosity measurements.

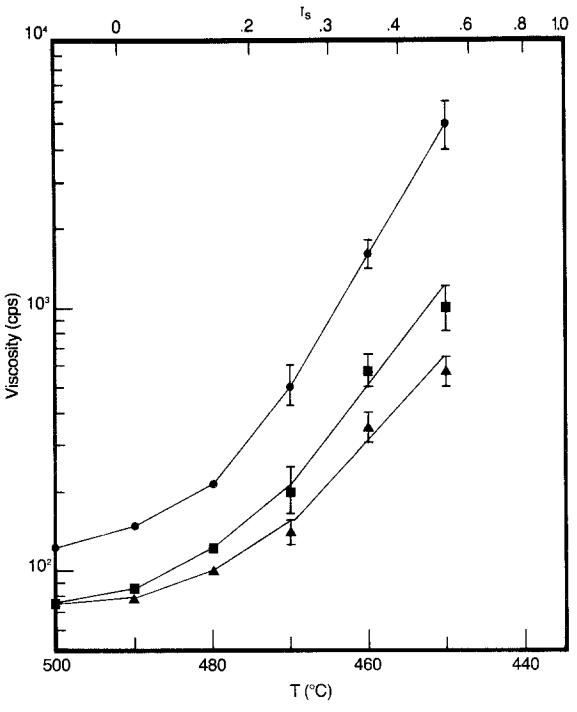

Figure 3 Apparent viscosity of ZA-27 alloy as a function of the temperature and the shear rate: • 152 rpm, $\dot{\gamma} = 125\,\text{sec}^{-1}$, $G = 1.25°\,\text{C min}^{-1}$; ▪ 360 rpm, $\dot{\gamma} = 300\,\text{sec}^{-1}$, $G = 1.09°\,\text{C min}^{-1}$; ▲ 760 rpm, $\dot{\gamma} = 640\,\text{sec}^{-1}$, $G = 1.0°\,\text{C min}^{-1}$.

within 1° C for an isothermal holding series. Fig. 3 shows the viscosity of ZA-27 slurries against the temperature and speed of the spindle. The cooling rate was constant during solidification of the alloys and ranged from 2.70 to 3.25° C min^{-1} respectively for the three imposed stirring speeds.

3.1. Apparent viscosity

At a very low stirring speed, for example 125 rpm, the apparent viscosity increased rapidly when the solidification started. This can be explained by the relatively low shear action of the stirrer at this speed. As shown in Fig. 4, the aluminium-enriched primary dendrites were not fragmented during solidification. Increasing the rotor speed decreased the viscosity of the slurries. In the range 360 rpm to 760 rpm, the apparent viscosity was remarkably constant until a solid fraction of 0.25 was formed, and apparent viscosities of less than 10 poises were observed in a slurry, with a solid fraction in excess of 0.50. This is consistent with experimental observations reported in earlier work [10]. The apparent viscosity can be expressed by an equation, describing the rearrangement of particles under shear, of the type:

$$\eta_a = A \exp [Bf_s] \qquad (1)$$

where η_a is the apparent viscosity and f_s the volume of solid fraction. The apparent viscosity of continuously cooled slurries of ZA-27 plotted on a semi-log scale shows a linear dependence on the solid fraction, as can be seen in Fig. 5. The values of coefficients A and B in Equation 1, calculated from Fig. 5, are listed in Table II. At high shear rates (i.e. 300 and $640\,\text{sec}^{-1}$), coefficient B was relatively constant and was respectively 2.74 for a shear rate of $300\,\text{sec}^{-1}$ and 2.27 for a shear rate of $640\,\text{sec}^{-1}$. At a low shear rate of $125\,\text{sec}^{-1}$, coefficient B was higher and was found to be 3.94. For all three regressions, the correlation coefficient r was close to 0.9.

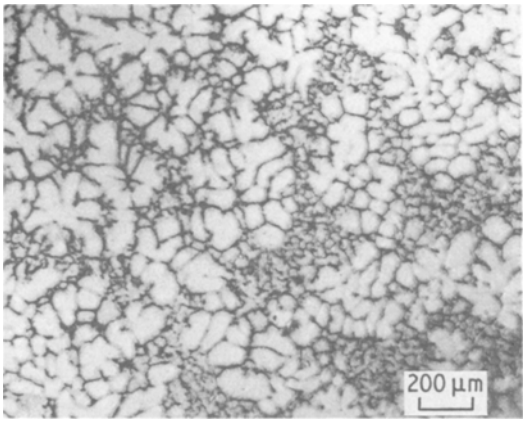

Figure 4 Micrograph of ZA-27 slurry sheared at 152 rpm and cooled to 0.30 solid fraction showing the dendritical structure.

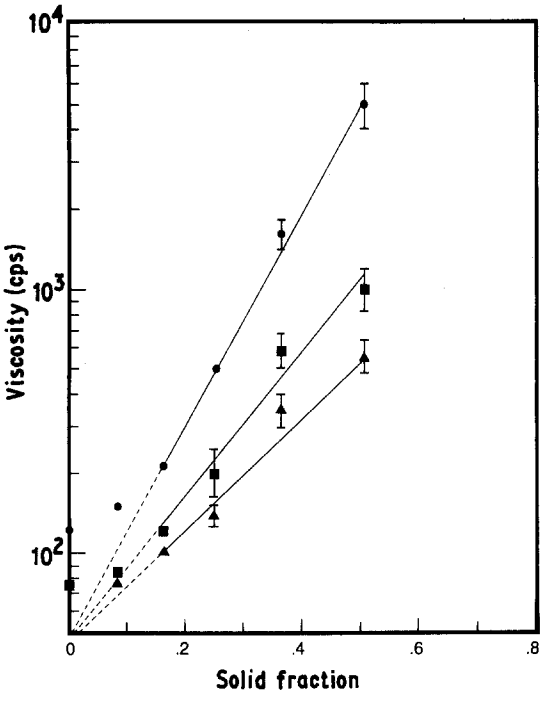

Figure 5 Apparent viscosity as function of solid fraction of ZA-27 slurries sheared continuously and cooled at a constant rate: • $\dot{\gamma} = 125\,sec^{-1}$; ▪ $\dot{\gamma} = 300\,sec^{-1}$; ▲ $\dot{\gamma} = 640\,sec^{-1}$.

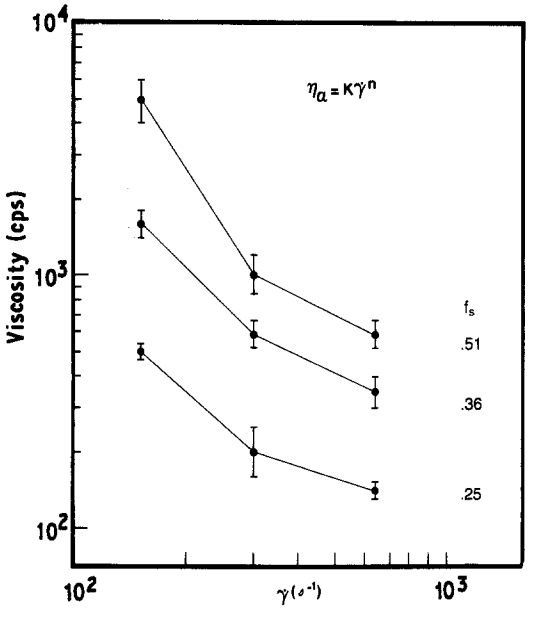

Figure 6 Apparent viscosity as a function of the shear rate of ZA-27 slurries at different solid fraction.

3.2. Effect of shear rate

The pseudoplasticity of stir-cast slurries can be expressed by a classical power-law equation, relating the flow behaviour of shear materials to the shear rate:

$$\eta_a = k\dot{\gamma}^n \qquad (2)$$

where $\dot{\gamma}$ is the shear rate and $0 < n < -1$ for a pseudoplastic material. Fig. 6 shows the apparent viscosity of ZA-27 slurries plotted on a log–log scale over the shearing range of different solid fraction. For high shear rates, values of n calculated for ZA-27 slurries range from -0.5 to -0.7 and are of the same order of magnitude as those reported for other alloy slurries [16, 18, 19]. At lower shear rates the slopes of our curves increase and display the viscosity behaviour of dendritical slurries.

TABLE II Experimentally determined coefficients of Equations 1 and 2 relating the apparent viscosity and the pseudoplasticity of ZA-27 alloy

Shear rate $\dot{\gamma}$ (sec^{-1})	Coefficients for Equation 1 $\eta_a = B\exp[Af_s]$
125	$\eta_a = 53\exp[3.94f_s]$
300	$\eta_a = 46\exp[2.74f_s]$
640	$\eta_a = 43\exp[2.27f_s]$

Vogel *et al.* [15] proposed that the effect of stirring was to transform the normal dendritic structure to one consisting of rounded primary particles owing to fragmentation of the dendrites. The grain boundaries are then fully wetted by the remaining liquid which assures the fluidity of the slurry. On the other hand, the high dependence of the viscosity on shear rate and cooling rate, which characterizes the thixotropic property of a stir-cast slurry, was pointed out by Flemings *et al.* [17, 18]. The primary particles formed by dendrite fragmentation caused to grow and cluster. This interacting phenomenon could be followed in isothermal studies.

3.3. Isothermal studies

In these experiments, the alloy was continuously sheared at a constant cooling rate until the desired slurry temperature was reached. The cooling rate was then brought to zero. The results of a typical isothermal viscosity experiment is shown in Fig. 7. Under shear rates of $640\,sec^{-1}$, the slurry was cooled from the melting point to 460° C (i.e. $f_s = 0.36$) then maintained there. The initial apparent viscosity of the slurry was 100 cps at 460° C. It reached 350 cps within 5 min of holding and then remained constant. Joly *et al.* [18] pointed out that the basic explanation of pseudoplasticity of

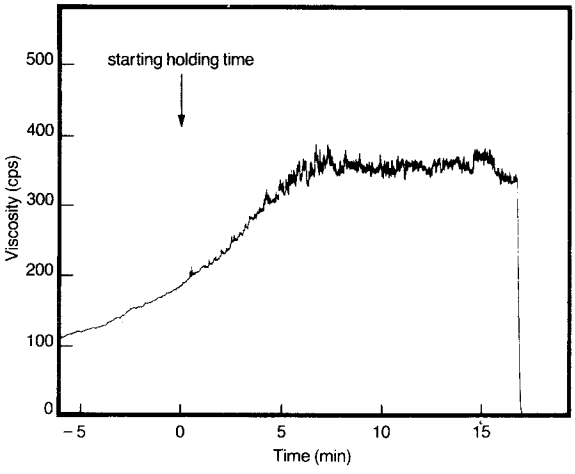

Figure 7 Apparent viscosity as a function of the shear rate of isothermal ZA-27 slurries sheared continuously and cooled at a constant rate.

metal slurries is based on an equilibrium between the rate of buildup and breakdown of the aggregated structure. The buildup is due to the particle growth and clustering effect and the breakdown is caused by the mechanical agitation.

4. Microstructural studies

Typical microstructures of conventional and stir-cast ZA-27 alloys are shown in Fig. 8. A sand-cast microstructure is presented in Fig. 8a showing usual α-phase dendrites bordered by an $\alpha + \eta$ eutectic phase. The structure of slurries solidified in a graphite mould is shown in Fig. 8b, where two distinctive solidification modes can be clearly seen. After pouring into the graphite crucible, solidification of the remaining liquid is accelerated producing a fine dendritic structure. It is apparent that primary particles are strongly cohesive with the matrix. During the secondary solidification phase, primary particles continue to grow through the liquid at the same time as other newly formed nucleons. As the cooling rate accelerates, the solidification interface is broken [20] forming little excrescences which form along all grain boundaries. Decreasing the cooling rate of the final (or secondary) solidification increases the size of

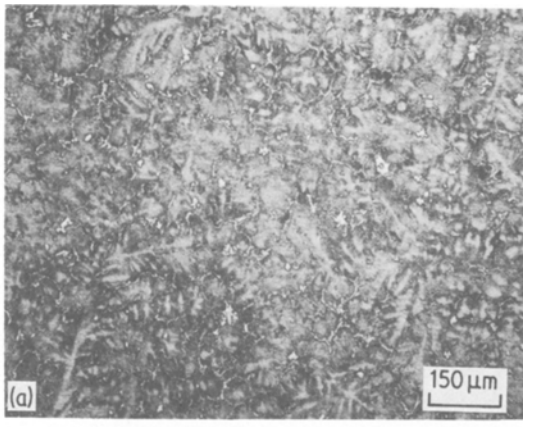

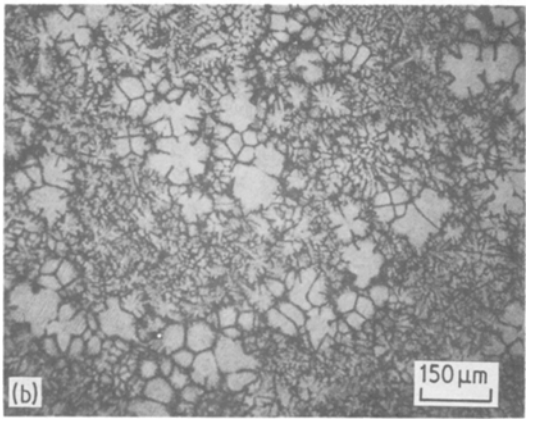

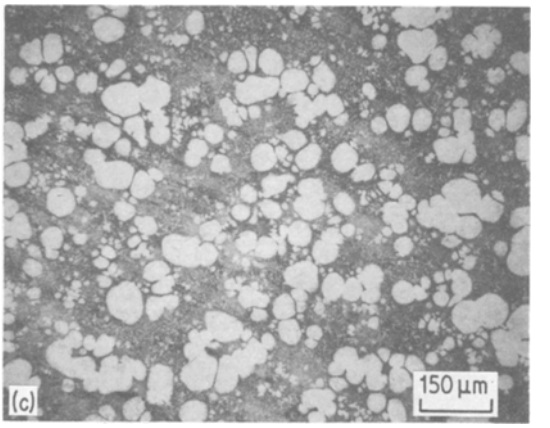

Figure 8 Microstructure of ZA-27 samples: (a) conventional sand-cast as received; (b) stir-cast alloy solidified at a solid fraction of 0.40 and poured into a graphite mould; (c) the same as (b) but water-quenched when delivered out of the stir-cast machine.

TABLE III Effect of casting temperature on the morphology of primary particles of continuous-cooling ZA-27 slurries

Temperature (°C)	$\%f_s$*	Morphology	Particles†			Clusters
			Density (ρ mm^{-2})	$\emptyset$ (μm)	σ (μm)	$\emptyset$ (μm)
485	12	Numerous nucleons < 5 μm, few particles of 20 μm max	–	–	–	–
480	15	Nucleons + spheroids	40	40	25	–
475	20	Nucleons + spheroids	70	35	25	–
470	25	Nucleons + spheroids	145	37	35	–
465	30	Nucleons + spheroids	125	32	30	–
460	35.7	Spheroids + rosettes + clusters	95	37	30	100–200
455	42.6	Coarser rosettes + clusters	115	55	20	150–200
450	51.2	Coarser rosettes + clusters	100	65	30	150–200
445	62.5	Branched rosettes + clusters	120	70	35	200–300

Note: The stirring speed was constant at 600 rpm (equivalent to $\dot{\gamma} = 500\,\text{sec}^{-1}$).
*The solid fraction was calculated from the solidus and liquidus curves.
†Only the particles with a diameter > 5 μm were counted.
$\emptyset$ The average diameter of particles or clusters.
σ The standard error and indicates the distribution of particle size.

secondary particles. The distinction between the two types of particles becomes difficult to make when the two cooling rates (primary and secondary) are of the same order of magnitude, particularly when the morphology of dendrites of the studied alloys is coarse and round as in Al–Cu alloys [21].

The identification of the original morphology is easier for directly quenched specimens. This can be seen in Fig. 8c, where, spheroidized particles already formed in the slurry machine are clearly delineated from the remaining liquid which solidified on quenching. A large particle size distribution is observed throughout the specimens. There is also a clear tendency for particles to agglomerate in a clustered formation. In order to follow the different mechanisms which govern the formation of this particular microstructure, a series of specimens were prepared by varying the temperature and maintaining all other variables constant.

4.1. Effect of temperature

For these series of tests, the cooling rate and the shear rate were kept constant at respectively $1°\,\text{C}\,\text{min}^{-1}$ and $500\,\text{sec}^{-1}$. Table III gives changes in the morphology of primary particles produced by a change in temperature. Fig. 9 illustrates some of these microstructures along with the temperatures at which they were produced. When the solid fraction is below 0.15, the microstructure shows a high concentration of nucleons of less than 5 μm with a few coarse particles of less than 20 μm disseminated throughout the matrix, as shown in Fig. 7a. When the temperature was decreased, the primary particles became coarser. Statistical measurements of particle size and their distribution show that the average diameter is relatively constant until the solid fraction exceeds 0.35. The increase of the solid fraction is principally due to enhanced nucleation. With a solid fraction above, 0.35, more rosettes were formed with a clear tendency to cluster, as shown in Fig. 9b. The average diameter of particles increased, denoting the coalescence of particles. Up to a solid fraction of 0.60 the rosettes have more branches, and the clusters are found to be larger. Typical clusters contain 15 to 30 individual particles and have a diameter of 200 to 300 μm, as shown in Fig. 9c. Fig. 10 shows the average diameter of primary particles as a function of temperature, with histograms of particle size. In this evaluation, only particles bigger than 5 μm were measured; the smaller ones were numerous and could have been confused with the secondary particles.

The morphology changes described above demonstrate the complexity of the mechanisms of formation of stir-cast structures. At the start of solidification, nucleation followed by particle growth and mechanical fragmentation can explain the microstructural features observed. But as solidification progresses, the clustering tendency of primary particles becomes important and changes the microstructure by promoting the formation of larger particles (rosettes), bonded

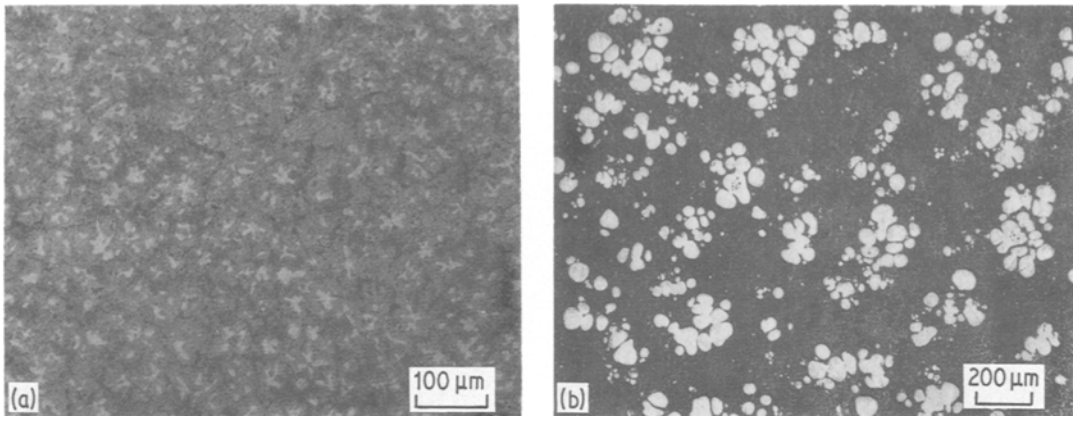

Figure 9 Microstructure of stir-cast ZA-27 alloy at different temperatures: (a) solidified at a solid fraction of 0.15 showing the nucleation of primary particles; (b) solidified at a solid fraction of 0.30 showing rosettes and bonded particles; (c) solidified at a solid fraction of 0.50 showing clusters.

particles and unbounded groups, as shown in Fig. 9c. Rosettes with bends, necks or branches are due to the coalescence and sintering of primary particles [22]. The observation of "special boundaries" in stir-cast Al–Mg alloys [16] favours the theory of a coalescence mechanism for the formation of large primary particles. For bonded particles, Prasad *et al.* [21] had proposed a particle collision phenomenon producing interparticle bonds. The sintering effect eventually transforms the bonds to necks; then growth of the necks leads to the formation of rosettes or particles of larger size. The method, described by Apaydin *et al.* [16] involving microanalysis of the solute distribution across the observed particle boundaries, can be used to support the recrystallization mechanism. Nevertheless, the mechanisms proposed above explain only the behaviour of clustered particles or at least colliding particles, but the reason for the tendency of primary particles to cluster is not clear. Assar *et al.* [23] revealed that particle agglomeration does not disappear when shear rate increases; it only becomes smaller. It is

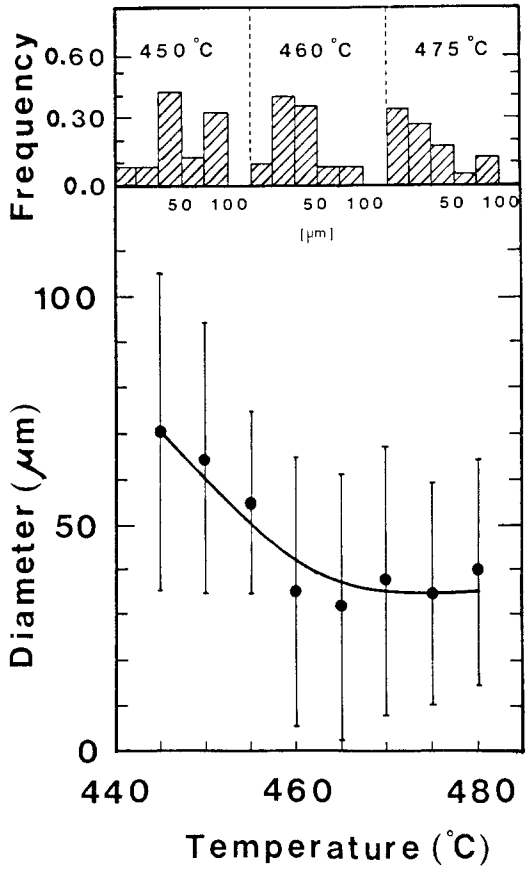

Figure 10 Size distribution of primary solid particles in ZA-27 samples sheared continuously and cooled at a constant rate to different casting temperatures.

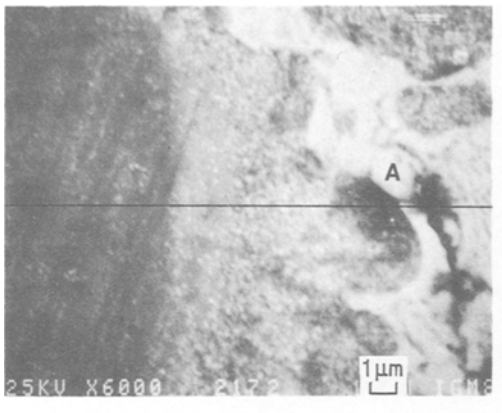

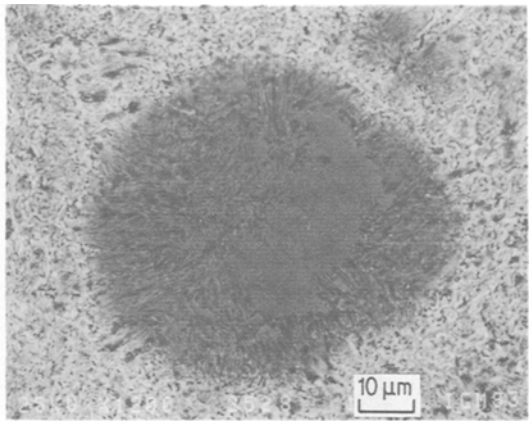

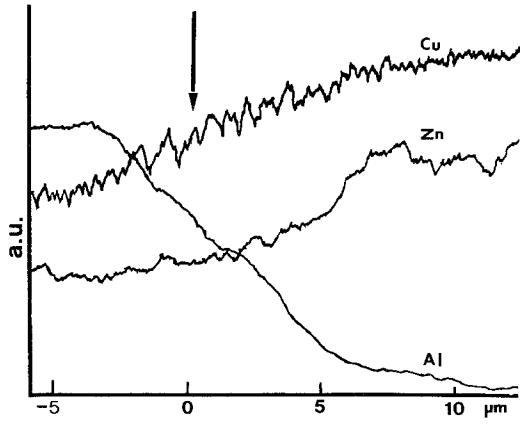

Figure 11 Electron microprobe analysis showing the composition variation through an interface of a primary particle and the remaining liquid.

Figure 12 Enlarged electron micrograph of a primary particle showing radial lamellar structure ($\alpha + \eta$).

tempting, though, to explain this feature by the necessity of sheared slurry to reach the lowest possible viscosity. Joly *et al.* [18] have introduced the notion of liquid retention between particles. At the start of solidification when the solid fraction is not important, the density and the average size of particles are not obstacles to the flow of the slurry. But as solidification progresses, the remaining liquid becomes less important and part of it is entrapped between coarser particles. In this case, a decrease of interparticle space reduces the amount of entrapped liquid, thus the remaining liquid can move more easily around the agglomeration.

Work is currently in progress to understand the influence of high shear rates and high cooling rates on stir-cast solidification. Studies of other alloys also help to shed more light on this phenomenon.

4.2. Microsegregation analysis

In spite of the clustering effect of primary particles which modifies only the low range size distribution, the microstructure of stir-cast ZA-27 alloys was found to be homogenous throughout the ingot. A typical composition profile of alloy elements, obtained by electron-probe analysis through a particle–liquid interface is shown in Fig. 11. The primary particles exhibit a remarkably flat concentration profile rich in Al with a concentration of approximately 60 wt % Al. A small solute enrichment at the edge of the particles was observed, due to the accelerated rate of solidification. This is a characteristic feature of a stir-cast alloy [24] and may be attributed to the steady-state growth of primary particles. The remaining liquid, rich in zinc and copper, solidifies as dendrites with formation of an $\alpha + \eta$ eutectic phase between the dendrite arms. Copper is found to be segregated out of the phase and is precipitated in the form of ϵ-phase $CuZn_4$ rich in zinc and copper. The morphology of these precipitates is coarse and round and was easily observed (Fig. 11, mark A). Elsewhere, the phase formed at high temperature exhibits an eutectoid transformation at 275°C as can best be seen on the enlarged micrograph of a primary particle (Fig. 12). The lamellar structure ($\alpha + \eta$) obtained by the decomposition of the α-phase starts at the edge of the particles and progresses radially towards their centres.

This particular microsegregation can also be illustrated by microhardness measurements. Primary particles show a Vickers hardness in the range of 105 to 110. The matrix or remaining liquid is harder with a HVN in the range of 120 to 130. Finally, the global hardness of stir-cast ZA-27 alloy was measured with a Rockwell

hardness tester. The values of Rockwell hardness 60 kg measured across the ingots are in the range of 84 to 90 and are similar to those measured on sand-cast alloys.

5. Conclusions

Stir-cast Zn–27 wt% Al was successfully cast in the range of 0.2 to 0.6 solid fraction. With shear rates from 300 to 640 sec^{-1}, the continuously cooled slurries showed a structure composed of spherical or rosette-shaped particles suspended in the remaining liquid. The apparent viscosity was less than 10 poises and followed the classical power-law equation, describing the flow behaviour of pseudoplastic shear materials. At lower shear rates, the primary particles were more dendritic and the apparent viscosity increased.

Microsegregation analysis showed that primary particles are made up of α-phase. The copper is segregated in the interparticle zone. Morphology studies revealed a clear tendency of primary particles to cluster. This effect which acts in the opposite way to the shearing force, became predominant when the temperature was lowered. The clustering phenomenon could be explained by the reduction of the amount of entrapped liquid in the particles.

Acknowledgements

The authors would like to express their appreciation to R. Lavallée for his technical assistance, and their acknowledgements to Dr J.-J. Hechler for the thermodynamic property measurements and to Dr S. Dallaire for the plasma-sprayed work.

References

1. N. A. EL-MAHALLAWY, N. FAT-HALLA and M. A. TAHA, in Proceedings of the 4th International Conference on Mechanical Behaviour of Materials, Stockholm, Sweden, 1983, edited by J. Carlsson and N. G. Ohlson (1983) p. 695.
2. A. ASSAR, N. A. EL-MAHALLAWY and M. A. TAHA, *Aluminium* 57 (1981) 807.
3. F. J. KIEVITS and K. V. PRABHAKAR, in Proceedings of the International Symposium on "Quality Control of Engineering Alloys and the Role of Metal Science", Delft, Delft University of Technology, The Netherlands, 1977) p. 203.
4. F. C. BENNETT, T. E. LEONTIS and S. L. COULING, in Proceedings of the 34th Annual Meeting of the International Magnesium Association, (International Magnesium Association, Bayton, Ohio, 1977) p. 23.
5. E. F. FASCETTA, R. G. RIEK, R. MEHRABIAN and M. C. FLEMINGS, *AFS Cast Metals Res. J.* 9 (1973) 167.
6. R. G. RIEK, A. VRACHNOS, K. P. YOUNG, N. MATSUMOTO and R. MEHRABIAN, *AFS Trans.* 19 (1975) 25.
7. J. M. OBLAK and W. H. RAND, *Met. Trans. B.* 7B (1976) 699.
8. K. P. YOUNG, R. G. RIEK and M. C. FLEMINGS, *Metal. Technol.* 4 (1979) 130.
9. C. C. LAW, J. D. HOSTETLER and L. F. SCHULMEISTER, *Mater. Sci. Eng.* 38 (1979) 123.
10. K. P. YOUNG, R. G. RIEK and M. C. FLEMINGS, "Solidification and Casting of Metals" (The Metals Society, London, 1979) p. 510.
11. M. C. FLEMINGS, R. G. RIEK and K. P. YOUNG, *Mater. Sci. Eng.* 25 (1976) 103.
12. S. RAMATI, G. ABBASCHIAN and R. MEHRABIAN, *Met. Trans. B.* 9B (1978) 241.
13. R. MEHRABIAN and M. C. FLEMINGS, *AFS Trans.* 80 (1972) 173.
14. M. C. FLEMINGS and R. MEHRABIAN, in Proceedings of the 40th International Foundry Congress 1973, Moscow, No. 15.
15. A. VOGEL, R. D. DOHERTY and B. CANTOR, "Solidification and Casting of Metals" (The Metals Society, London, 1979) p. 518.
16. N. APAYDIN, K. V. PRABHAKAR and R. D. DOHERTY, *Mater. Sci. Eng.* 46 (1980) 145.
17. M. C. FLEMINGS, R. G. RIEK and K. P. YOUNG, *AFS Int. Cast. Metal. J.* 3 (1976) 11.
18. P. A. JOLY and R. MEHRABIAN, *J. Mater. Sci.* 11 (1976) 1393.
19. J. COLLOT, *Mèmoires Et. Sci. Rev. Met.* 9 (1983) 440.
20. Rheocasting, in Proceedings of a workshop held at the AMMRC (1977), MCIC Report Columbus, Ohio.
21. P. R. PRASAD, S. RAY, J. L. GAINDHAR and M. L. KAPOOR, *Z. Metallkde.* 73 (1982) 714.
22. A. VOGEL, *Met. Sci.* 12 (1978) 576.
23. A. ASSAR, N. EL-MAHALLAWY and M. A. TAHA, *Met. Technol.* 9 (1982) 165.
24. T. Z. KATTAMIS, in Proceedings of the International Symposium, Delft (Delft University of Technology, 1977) p. 189.

Received 14 February
and accepted 9 March 1984